

# $\mathcal{PT}$ -Symmetric Waveguides With Tunable Parameters

Chao Hang, Dmitry A. Zezyulin, Guoxiang Huang, and Vladimir V. Konotop

(Invited Paper)

**Abstract**—We propose a physical setting for a  $\mathcal{PT}$ -symmetric waveguide with spatially varying parameters and mode structure. The system consists of a mixture of isotopes of Rubidium  $\Lambda$ -atoms loaded in a cell with Bragg cladding and exposed to laser fields ensuring Raman excitations, controlling the real and imaginary parts of the refractive index of the system. It is shown that the system parameters can be designed to support different numbers of propagating modes in different parts of the waveguide as well as to create localized defects. We study the wave transition between different waveguide configurations. We address two types of defects in more details: 1) tunable defects, which are related to the variation of the refractive index inside the waveguide, and 2) fixed defects created by changes of a Bragg cladding. We demonstrate that the change of the waveguide toward the increase of the number of guided modes can support and even enhance the light propagation. However, if a transition, or a defect, results in a reduction of the number of guiding modes, strong attenuation of guided beams can be observed. As a result, the proposed waveguides may support unidirectional propagation of light and operate as switches and amplifiers.

**Index Terms**—Defects, optical waveguides, parity-time symmetry, unidirectional light propagation.

## I. INTRODUCTION

COHERENT atomic gases are promising candidates for achieving many important optical functionalities not available in naturally occurring systems. Properties of dispersion and absorption of a coherent atomic gas can be modified and actively manipulated by using pump and control laser fields, which have been used to realize slow lights [1], enhanced parametric processes [2], light memory [3], [4], and to obtain large optical refractive indices without absorption [5]–[7], etc. Recently, it has been shown that parity-time ( $\mathcal{PT}$ )-symmetric refractive

index can be realized in coherent atomic systems with three-level or four-level configurations [8]–[12].

$\mathcal{PT}$  symmetry implies that the real part of the refractive index  $n(x)$ , i.e.,  $\text{Re}[n(x)]$ , which represents phase shift, must be even, while the imaginary part of the refractive index, i.e.,  $\text{Im}[n(x)]$ , which represents loss or gain, must be odd. The constraint,  $n(x) = n^*(-x)$ , guarantees stable propagation of linear modes in a medium with gain and dissipation [13], provided that the  $\mathcal{PT}$  symmetry is unbroken, i.e., the spectrum of underlying linear eigenvalue problem is all-real (if the spectrum contains complex eigenvalues, then  $\mathcal{PT}$  symmetry is said to be broken [14], [15]).  $\mathcal{PT}$ -symmetric systems based on atomic gases interacting with laser fields possess great advantages since they may have authentic  $\mathcal{PT}$ -symmetric refractive indexes, i.e., balanced gain and loss in the whole space, and can be easily controlled *in situ* with high precision through an active adjustment of system parameters. We also note that the idea of using active two-level atoms, described by the Lorentz model [16], was exploited in [17] for modeling the pulse propagation through a  $\mathcal{PT}$ -symmetric layer. Actively doped materials were used in experiments where various aspects of the  $\mathcal{PT}$ -symmetry breaking [18]–[20] were studied.

Spontaneous  $\mathcal{PT}$ -symmetry breaking appears to be an efficient mechanism for unidirectional, reflectionless (invisible) propagation of light [21]–[23], where the reflection from one side of a device is significantly suppressed compared to propagation in the opposite side, as well as the non-reciprocity, when nonlinearities are involved [19], [20]. Although  $\mathcal{PT}$ -symmetry breaking is an essential ingredient for modeling and experimental observation, unidirectional light propagation can be also implemented in purely conservative media, say, by using anisotropic band-gap structures [24], [25], nonlinear  $\chi^{(2)}$  media in photonic crystals [26], or properly engineered asymmetric shapes of nonlinear materials [27]. An optical diode based on a moving photonic crystal was recently created experimentally in a medium with three-level atoms via electromagnetically induced transparency [28]. Apart from different frequency domains, the main physical distinction between the  $\mathcal{PT}$ -symmetry-based schemes and the conservative schemes resides in the possibility of flexible control offered by gain-and-loss mechanism in the former ones, and the absence of gain or attenuation in the latter ones.

In this article, we propose a new physical scheme to produce a  $\mathcal{PT}$ -symmetric optical waveguide for realizing a unidirectional propagation of light. Our system consists of a mixture of two isotopes of Rubidium (Rb) atomic gas with

Manuscript received November 29, 2015; revised February 21, 2016; accepted February 23, 2016. Date of publication March 11, 2016; date of current version May 19, 2016. The work of C. Hang and G. Huang was supported by NSF-China under Grant 11475063, 11174080, and 11474099. The work of D. A. Zezyulin and V. V. Konotop was supported by the FCT (Portugal) under Grant PTDC/FIS-OPT/1918/2012.

C. Hang and G. Huang are with the State Key Laboratory of Precision Spectroscopy and the Department of Physics, East China Normal University, Shanghai 200062, China, and also with the NYU-ECNU Joint Institute of Physics, New York University Shanghai, Shanghai 200062, China (e-mail: chang@phy.ecnu.edu.cn; gxhuang@phy.ecnu.edu.cn).

D. A. Zezyulin and V. V. Konotop are with the Centro de Física Teórica e Computacional and Departamento de Física, Faculdade de Ciências, Universidade de Lisboa, Lisboa 1749-016, Portugal (e-mail: d.zezyulin@gmail.com; vvkonotop@fc.ul.pt).

Color versions of one or more of the figures in this paper are available online at <http://ieeexplore.ieee.org>.

Digital Object Identifier 10.1109/JSTQE.2016.2537218

$\Lambda$ -type three-level configuration, loaded in a cell with Bragg cladding and exposed to (probe, pump, control, and Stark) laser fields with Raman excitations. We show that the real and imaginary parts of the refractive index  $n(x)$  can be easily manipulated and a  $\mathcal{PT}$ -symmetric  $n(x)$  can be realized. We demonstrate that through modulating system parameters such  $\mathcal{PT}$ -symmetric waveguide allows transitions between waveguide configurations and hence supports different numbers of guiding modes. From the perspective of manipulating the system properties, we consider two types of transitions, which includes a tunable one related to the local change of refractive index inside the waveguide, and a fixed one created by the change of the property of the Bragg cladding. Such transitions can be implemented in a finite region of propagation distance through introduction of suitable defects. We find that the change of the waveguide towards an increase of the number of guiding modes can support and even enhance light propagation. However, if a transition or a defect results in a reduction of the number of guiding modes, a strong attenuation of guided beams may be observed. As a result, the  $\mathcal{PT}$ -symmetric optical waveguide with these defects can be used to design optical diodes, switches, and amplifiers.

The article is arranged as follows. Section II describes the realization of the  $\mathcal{PT}$ -symmetric refractive index by using a coherent atomic gas. Section III studies the tunable and fixed transitions and defects in the waveguide with  $\mathcal{PT}$  symmetry. Section IV explores passages between one- and two-mode waveguides and the possibility of realizing optical diode-like devices. Sections V, VI, and VII discuss the scattering by defects of different kinds which create localized modifications of the mode structure of the waveguide, respectively. The last section (i.e., Section VIII) summarizes the main results obtained in this work.

## II. $\mathcal{PT}$ SYMMETRY BASED ON AN COHERENT ATOMIC GAS

We start with a practical physical system reported in [8], which contains two species of atoms, i.e., isotopes of  $^{87}\text{Rb}$  (species 1) and  $^{85}\text{Rb}$  (species 2). Each species of atoms has a  $\Lambda$ -type level configuration and is embedded into a one-dimensional (1-D) photonic crystal waveguide (see Fig. 1). A weak probe field  $\mathbf{E}_p$  (strong control field  $\mathbf{E}_c$ ), propagating along the  $z$ -direction with wavenumber  $k_p$  ( $k_c$ ) and angular frequency  $\omega_p$  ( $\omega_c$ ), drives the ground state  $|g, s\rangle$  ( $|a, s\rangle$ ) to the excited level  $|e, s\rangle$  ( $s = 1, 2$  indicates the species of the atoms). For the mixture of Rb isotopes we assign  $|g, s\rangle = |5S_{1/2}, F = 1\rangle$ ,  $|a, s\rangle = |5S_{1/2}, F = 2\rangle$ , and  $|e, s\rangle = |5P_{1/2}, F = 0\rangle$ . The half Rabi frequency of the probe field (control field) is defined as  $\Omega_p = |\mathbf{e}_p \cdot \mathbf{p}_{eg}|E_p/(2\hbar)$  ( $\Omega_c = |\mathbf{e}_c \cdot \mathbf{p}_{ea}|E_c/(2\hbar)$ ), where  $\mathbf{p}_{eg}$  ( $\mathbf{p}_{ea}$ ) is electric dipole matrix elements associated with the transition  $|e, s\rangle \leftrightarrow |g, s\rangle$  ( $|e, s\rangle \leftrightarrow |a, s\rangle$ ) and is assumed to be approximately equal for both isotopes. For the selected levels of Rb atoms,  $p_{eg} \approx p_{ea} = 10^{-27} \cdot 2.54 \text{ C} \cdot \text{cm}$  [29].  $\mathbf{e}_p$  and  $E_p$  ( $\mathbf{e}_c$  and  $E_c$ ) are, respectively, the polarization unit vector and envelope of the probe field (control field).

The probe-field susceptibility outside the atomic cell can be found as the effective refractive index of the Bragg cladding  $\chi_{\text{clad}}$ . Inside the atomic cell, it is defined by  $\chi_p = p_{eg}^2(N_1\rho_{eg}^1 +$

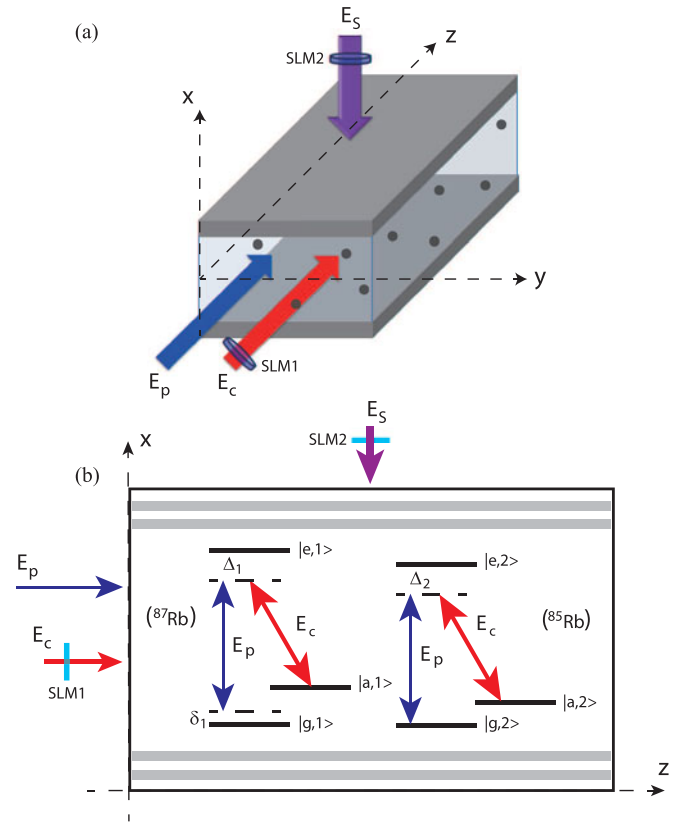


Fig. 1. (a) Possible 3-D arrangement for the suggested system. The probe field  $E_p$ , polarized in  $y$ -direction, and the control field  $E_c$  propagate along the  $z$  axis. The Stark field  $E_s$  propagates along the  $x$  axis. The gray slabs denote the photonic crystal (Bragg mirrors). The black points indicate the volume filled in by the atomic gas. SLM1 and SLM2 denote the spatial light modulators for the Stark field and the control field, necessary for creating desirable spatial profile of the field. (b) Energy-level diagram and Raman resonance scheme of the mixture of two three-level  $\Lambda$  systems.  $\Delta_s$  ( $s = 1, 2$ ) are the one-photon detunings, while  $\delta_1$  is the two-photon detuning. The gray stripe denotes the photonic crystal.

$N_2\rho_{eg}^2)/(\epsilon_0\hbar\Omega_p)$ , where  $N_s$  is the density of the  $s$ th isotope. The atomic coherence  $\rho_{eg}^s$  of the  $s$ th isotope can be computed from the Bloch equations [30] and in our case it leads to the susceptibility of the form [8]:

$$\chi_p = \frac{p_{eg}^2}{\epsilon_0\hbar}(N_1D_1 + N_2D_2) \quad (1)$$

with  $D_1 = \delta_1/[\delta_1(\delta_1 + \Delta_1 - i\Gamma) - |\Omega_c|^2]$  and  $D_2 = 1/(\Delta_2 + i\Gamma)$ . Here  $\Delta_s = \omega_e^s - \omega_a^s - \omega_c$  and  $\delta_s = \omega_a^s - \omega_g^s - (\omega_p - \omega_c)$  are, respectively, one- and two-photon detunings, with  $\omega_a^s$  ( $\omega_g^s$ ) denoting the eigenfrequency of level  $|a, s\rangle$  ( $|g, s\rangle$ ) and  $\delta_2 \approx 0$ . In addition,  $\Gamma = \Gamma_{eg} \approx \Gamma_{ea}$  with  $\Gamma_{eg}$  ( $\Gamma_{ea}$ ) denoting the spontaneous-emission decay rate from  $|e, s\rangle$  to  $|g, s\rangle$  (from  $|e, s\rangle$  to  $|a, s\rangle$ ). The spontaneous-emission decay rate from  $|a, s\rangle$  to  $|g, s\rangle$  is much smaller than  $\Gamma$  and hence can be neglected, i.e.,  $\Gamma_{ag} \approx 0$ . For cold and dilute Rb atoms  $\Gamma \approx \pi \times 5.75 \text{ MHz}$ , and the dephasing process can also be neglected [29].

The spatial distribution of the  $\mathcal{PT}$ -symmetric probe-field susceptibility (and thus of the refractive index  $n \approx \sqrt{1 + \chi_p}$ ,  $\chi_p(x) = \chi_p^*(-x)$  [ $n(x) = n^*(-x)$ ], can be obtained by apply-

ing an additional far-detuned laser field, i.e., the Stark field (see e.g. [30]),  $E_S(x) \cos(\omega_S t)$ , which induces energy shifts of levels  $|j, s\rangle$ ,  $\Delta E_{j,s}(x) = -\alpha_j E_S^2(x)/4$  with  $\alpha_j$  being the scalar polarizability. In addition, the control field is assumed to be  $x$ -dependent, i.e.,  $\Omega_c = \Omega_c(x)$ . For the selected levels of Rb atoms,  $\alpha_e - \alpha_g \approx 2\pi\hbar \cdot 0.1223 \text{ Hz}(\text{cm}/\text{V})^2$  and  $\alpha_g \approx \alpha_a$  [29]. Thus  $\Delta_s(x) = \Delta_s - (\alpha_e - \alpha_g)E_S^2(x)/(4\hbar)$ , whereas  $\delta_1$  is not  $x$ -dependent. Note that the characteristic scale of the  $\Delta_s(x)$  modulation is comparable to the Stark-field wavelength  $\lambda_S$ .

The evolution of the probe-field Rabi frequency  $\Omega_p$  under paraxial approximation [30] is given by

$$i \frac{\partial \Omega_p}{\partial \zeta} + \frac{\partial^2 \Omega_p}{\partial \xi^2} + \frac{k_p^2}{2k_S^2} \chi_p(\xi) \Omega_p = 0, \quad (2)$$

with  $\zeta = (k_S^2/k_p)z$  and  $\xi = \sqrt{2}k_S x$  ( $k_S = 2\pi/\lambda_S$ ). The second term on the left hand side of Eq. (2) describes the diffraction of the probe beam in the  $x$  direction.

We are interested in the  $\mathcal{PT}$ -symmetric profile of the first-order probe-field susceptibility with a parabolic real and linear imaginary parts in the atomic cell, i.e.,

$$\chi_p(\xi) \approx \begin{cases} \tilde{\chi}_0 + i\tilde{\chi}_1\xi + \tilde{\chi}_2\xi^2, & |\xi| \leq 1, \\ \chi_{\text{clad}}, & |\xi| > 1. \end{cases} \quad (3)$$

Using the transformation  $\Omega_p = \Omega_0 q e^{i[k_p^2 \tilde{\chi}_0 / (2k_S^2)]\zeta}$  ( $\Omega_0$  is the typical Rabi frequency of the probe field) and expression (1), we obtain the dimensionless equation

$$i \frac{\partial q}{\partial \zeta} + \frac{\partial^2 q}{\partial \xi^2} + (iV_1\xi + V_2\xi^2)q = 0, \quad |\xi| \leq 1, \quad (4)$$

$$i \frac{\partial q}{\partial \zeta} + \frac{\partial^2 q}{\partial \xi^2} + V_0q = 0, \quad |\xi| > 1, \quad (5)$$

with  $V_{1,2} = \frac{k_p^2}{2k_S^2} \tilde{\chi}_{1,2}$  and  $V_0 = \frac{k_p^2}{2k_S^2} (\chi_{\text{clad}} - \tilde{\chi}_0)$ .

In what follows, we focus on a set of realistic parameters:  $\Delta_1 = 8\Gamma$ ,  $\Delta_2 = 8.72\Gamma$ ,  $\delta_1 = 1.81\Gamma$ , and  $\lambda_S = 10 \mu\text{m}$  (the waveguide width is considered to be of order of a few  $\lambda_S$ ). The electric dipole matrix element is  $p_{\text{eg}} = 2.5377 \times 10^{-27} \text{ C} \cdot \text{cm}$  [29]. The atomic densities of the first and second isotopes are  $N_1 \approx 2.62 \times 10^{13} \text{ cm}^{-3}$  and  $N_2 \approx 5.65 \times 10^{13} \text{ cm}^{-3}$ , respectively. With the above parameters, we obtain that  $\tilde{\chi}_0 \approx 0.46$ . In addition, we choose the effective susceptibility for the Bragg cladding  $\chi_{\text{clad}} \approx 0.45$ . Thus, we are dealing with the weak guidance because  $|\tilde{\chi}_0 - \chi_{\text{clad}}| \sim 10^{-2} \chi_{\text{clad}}$ .

Using the method described in Ref. [8], the model (4) can be realized by using the control and Stark fields shaped as

$$\Omega_c(\xi)/\Gamma = 2.553 - 0.276V_1\xi + 0.017V_2\xi^2, \quad (6)$$

$$E_S(\xi)/E_0 = 0.970 + 0.185V_1\xi - 0.074V_2\xi^2, \quad (7)$$

with  $E_0 = 10^4 \text{ V} \cdot \text{cm}^{-1}$ . Being focused onto a spot with a radius  $\sim 10\lambda_S \approx 0.1 \text{ mm}$ , the Stark field requires laser power  $\approx 12.5 \text{ W}$  (notice that this power is one-order smaller than the one required in Ref. [8], and can be achieved by using, say, quantum cascade lasers operating in mid-infrared wavelength range [31]). The spatial modulations of the control and Stark fields (6) and (7) can be created by using high-resolution spatial

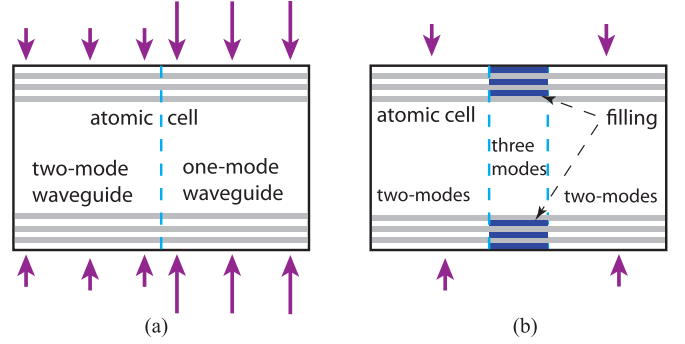


Fig. 2. Schematic of two types of transitions and examples for the modifications of wave guidance. (a) A tunable transition created by applying two different Stark fields (illustrated by different domains of the cell implements a switching from the two-mode to the one-mode regime (or vice versa). (b) A pair of fixed transitions, created by changing locally the effective refractive index of the cladding by filling with dielectric having a desired refractive index (shown by blue stripes), implements a fixed defect corresponding to a localized three-mode segment embedded into a two-mode waveguide. In both panels, vertical dashed lines show the location of the transitions [in the text, the corresponding positions are denoted by  $\zeta_0$  in Eq. (13) and by  $\zeta_0 - Z$  and  $\zeta_0 + Z$  in Eqs. (15), (17), (18), and (19)].

light modulators [32]. Since all lengths are scaled by  $\lambda_S$ , the pixel size of spatial light modulators should be much smaller than  $\lambda_S$ , say  $\sim 0.1\lambda_S \approx 1 \mu\text{m}$ .

It is also important to mention that in the expressions (6) and (7) we have preserved undetermined parameters  $V_1$  and  $V_2$ , which offers a possibility to tune the potential in a flexible way. In particular, the present system can be used to implement a single-mode waveguide if  $V_2 < 0$  [9], and a two-mode waveguide if  $V_2 > 0$  [10].

### III. TUNABLE AND FIXED TRANSITIONS AND DEFECTS

In this work, we are particularly interested in *transitions* between different guiding regimes which can be achieved by a change of the *effective* refractive index along the propagation direction, i.e., along  $\zeta$ . In an atomic cell, this can be achieved in two different ways, as illustrated in Fig. 2. First, a transition can be induced by tuning the control field and/or the Stark field [see Fig. 2(a)]. This leads to the change of the refractive index *inside* the atomic cell. Since the characteristics of the Stark field (like intensity or wavelength) in principle can be modified by weak detuning *in situ*, below we call this scenario a *tunable transition*. In this situation, the probe-field susceptibility is modeled by

$$\chi_p(\xi, \zeta) \approx \begin{cases} \tilde{\chi}_0 + i\tilde{\chi}_1(\zeta)\xi + \tilde{\chi}_2(\zeta)\xi^2, & |\xi| \leq 1, \\ \chi_{\text{clad}}, & |\xi| > 1, \end{cases} \quad (8)$$

where the expansion coefficients  $\tilde{\chi}_i(\zeta)$  are functions of  $\zeta$ .

Alternatively, one can consider *fixed* transitions introduced by variations of the cell attributes, like properties of Bragg mirrors (affecting  $\chi_{\text{clad}}$ ) [see illustration in Fig. 2(b)] or by geometry of the cell itself, which can be varying along the propagation. In this case

$$\chi_p(\xi, \zeta) \approx \begin{cases} \tilde{\chi}_0 + i\tilde{\chi}_1\xi + \tilde{\chi}_2\xi^2, & |\xi| \leq 1, \\ \chi_{\text{clad}}(\zeta), & |\xi| > 1. \end{cases} \quad (9)$$

As mentioned above, we are interested in transitions resulting in relatively strong perturbations of a waveguide, which involves a qualitative change of the mode structure. It is possible to suggest two implementations:

- 1) The transition changes the number of modes supported by the waveguide, but the  $\mathcal{PT}$ -symmetry of the entire configuration remains unbroken. For instance, an initially two-mode waveguide can undergo a transition to a one-mode or a three-mode regime.
- 2) The transition breaks the  $\mathcal{PT}$ -symmetry, i.e., several propagation constants become complex. This situation resembles recently studied interaction of a soliton in  $\mathcal{PT}$ -symmetric coupled nonlinear Schrödinger (NLS) equations with localized coupling defect [33], as well as soliton interaction with  $\mathcal{PT}$ -symmetric with a localized dissipative defect [34].

Notice that the change of the number of guided modes can be also realized in conservative waveguides (they correspond to  $V_1 = 0$ ). However, the transition to the complex propagation constants is specific to the  $\mathcal{PT}$ -symmetric (or, more generally, non-conservative) case.

As we will show below, a switching from the two-mode to the one-mode regime and the  $\mathcal{PT}$ -symmetry breaking can be designed using the tunable transition (8). On the other hand, a switching from the two-mode regime to a three mode regime can be implemented using the fixed transition (9).

Using two successive transitions, one can implement a *defect*, i.e., a localized modification of the guiding structure in a finite region of the propagation distance. Respectively, one can distinguished between tunable and fixed defects which can be designed using the transitions of different types. An example of a localized fixed defect is presented in Fig. 2(b).

#### A. Tunable Transition

Far from the transition, where the parameters of the waveguide are constant or change very slowly (i.e., can be considered adiabatically), one can look for a stationary mode in the form  $q(\xi, \zeta) = w(\xi)e^{ib\zeta}$ , where  $w(\xi)$  should be found from solution of the eigenvalue problem

$$bw = \frac{d^2 w}{d\xi^2} + U(\xi, \zeta)w, \quad (10)$$

where

$$U(\xi, \zeta) \approx \begin{cases} iV_1(\zeta)\xi + V_2(\zeta)\xi^2, & |\xi| \leq 1, \\ V_0, & |\xi| > 1, \end{cases} \quad (11)$$

which corresponds to the tunable transition (8). In Eqs. (10)–(11),  $\zeta$  should be considered as a parameter which governs the change of the coefficients  $V_1$  and  $V_2$ .

In order to identify the values of the parameters at which the structure of the spectrum changes, we will explore different combinations of the parameters  $(V_0, V_1, V_2)$  departing from the “default” combination  $(-1, 1.1, 10.5)$  which was elaborated in [10] and corresponds to the two-mode regime, i.e., exactly two distinct real eigenvalues in the discrete spectrum.

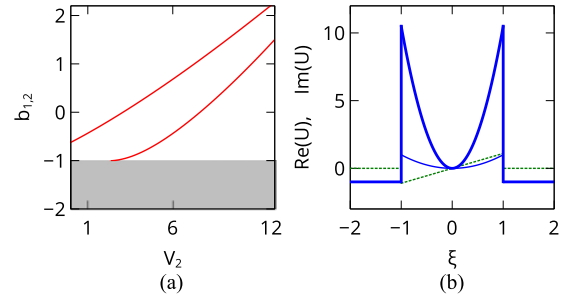


Fig. 3. Transition from two-mode regime to one-mode regime through the decrease of the parameter  $V_2$ . Panel (a) shows the isolated eigenvalues (one of which enters the continuous spectrum for  $V_2 \lesssim 2.5$ ). The shaded domain is occupied by the eigenvalues from the continuous spectrum. Solid lines in panel (b) show the real parts of the potential for  $V_2 = 10.5$  (bold blue line) corresponding to the two-mode regime and  $V_2 = 1$  (thin blue line) corresponding to the one-mode regime. The dashed line shows the imaginary parts of the refractive index which is the same in both the cases. In both panels,  $V_0 = -1$  and  $V_1 = 1.1$ .

First, we illustrate the possibility of the transition between two-mode and one-mode regimes. As shown in Fig. 3, this transition is achieved by decreasing the peak value of the real part of the refractive index. Mathematically, this is described by decreasing of the parameter  $V_2$ . As shown in Fig. 3(a), for sufficiently large  $V_2$  (say,  $V_2 = 10.5$ ) the waveguide supports exactly two real isolated eigenvalues and the continuous spectrum which occupies the real semi-infinite interval  $(-\infty, V_0)$ . At  $V_2 \approx 2.5$  the lowest propagation constant merges with the continuous spectrum. Physically, this is explained by the fact that the real part of the refractive index in the guiding domains becomes large with the increase of  $V_2$  and other parameters fixed [cf., bold and thin blue solid lines in Fig. 3(b)]. For instance, at  $V_2 = 1$  the system has exactly one isolated eigenvalue  $\approx -0.43$ . Notice that, for all values of the parameter  $V_2$  addressed in Fig. 3, the  $\mathcal{PT}$ -symmetry of the waveguide remains unbroken, and hence all propagation constants remain real even after the transition from the two-mode to the one-mode regime.

In order to observe another scenario, where both the guided modes become unstable passing through an exceptional point, we increase the imaginary part of the potential, i.e.,  $V_1$ . At the exceptional point, the two isolated eigenvalues coalesce forming a double eigenvalue. Upon the further increase of the gain-and-loss, the double eigenvalue splits into a pair of the complex conjugated ones, manifesting the spontaneous breaking of the  $\mathcal{PT}$ -symmetry. This scenario is illustrated in Fig. 4, where the exceptional point corresponds to  $V_1 \approx 1.5$ .

#### B. Fixed Transition

Turning now to the fixed transition of the type (9), we again consider eigenvalue problem (10), where the modulation of the refractive index is described by the following function

$$U(\xi, \zeta) \approx \begin{cases} iV_1\xi + V_2\xi^2, & |\xi| \leq 1, \\ V_0(\zeta), & |\xi| > 1, \end{cases} \quad (12)$$

where  $\zeta$  is considered as a parameter describing the cladding  $V_0$ . Computing the propagation constants for different values of  $V_0$ , we observe that the decrease of  $V_0$  to large negative values

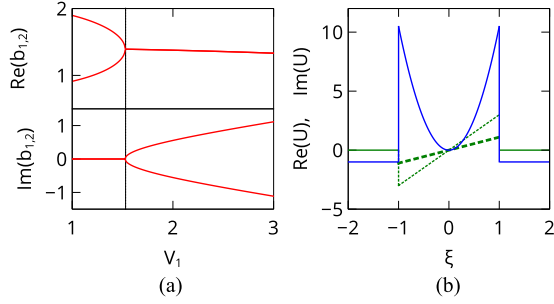


Fig. 4. Exceptional point and transition to broken  $\mathcal{PT}$ -symmetry by the increase of the parameter  $V_1$ . Panel (a) shows real (top) and imaginary (bottom) parts of the two isolated eigenvalues. Dashed lines in panel (b) show imaginary parts of the potential  $U(\xi, \zeta)$  for  $V_1 = 1$  (bold green line) corresponding to unbroken  $\mathcal{PT}$ -symmetry, and  $V_1 = 3$  (thin green line) corresponding to the broken  $\mathcal{PT}$ -symmetry. The solid line shows the real part of the refractive index which is the same in both the cases. In both panels,  $V_0 = -1$  and  $V_2 = 10.5$ .

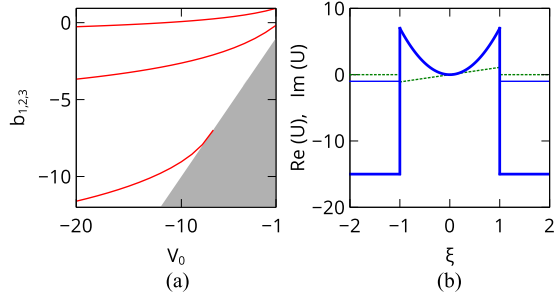


Fig. 5. Transition from two-mode regime to three-mode regime by changing the parameter  $V_0$ . Panel (a) shows the isolated eigenvalues (one of which emerges from the continuous spectrum at  $V_0 \approx -7$ ). The shaded domain is occupied by the eigenvalues from the continuous spectrum. Solid lines in panel (b) show the real parts of the potential for  $V_0 = -1$  (bold blue line) corresponding to the two-mode regime and  $V_0 = -15$  (thin blue line) corresponding to the three-mode regime. The dashed line shows the imaginary parts of the refractive index which is the same in both the cases. In both panels,  $V_1 = 1.1$  and  $V_2 = 7$ .

results in new isolated eigenvalues emerging from the continuous spectrum. This scenario is illustrated in Fig. 5. While for  $V_0 \gtrsim -7$  the waveguides supports exactly two isolated eigenvalues, it acquires three-mode structure for  $V_0 \lesssim -7$ .

#### IV. TRANSITION BETWEEN ONE- AND TWO-MODE WAVEGUIDES: UNIDIRECTIONAL PROPAGATION

First of all, in Fig. 6 we illustrate the stationary modes and their evolution in one-mode [see panels (a), (b)] and two-mode [see panels (c)–(f)] regimes of the waveguide. The stationary modes (left panels) are obtained by solving the eigenvalue problem (10), directly. The evolution of modes (right panels) is obtained by solving Eqs. (4) and (5) with the split-step Fourier method. Fig. 6(a) and (b) shows the mode and its evolution for the case where the waveguide carries exactly one mode. Fig. 6(c) and (e) shows two modes and their stable propagation [(e) and (f)] in a waveguide carrying two modes. Notice that one of the modes is fast [see Fig. 6(e)] with the propagation constant  $\approx 0.93$ , while the other mode is slow with the propagation constant  $\approx -0.17$ .

Now we turn to the dynamical regimes corresponding to the situation described by the model (4). For the sake of conve-

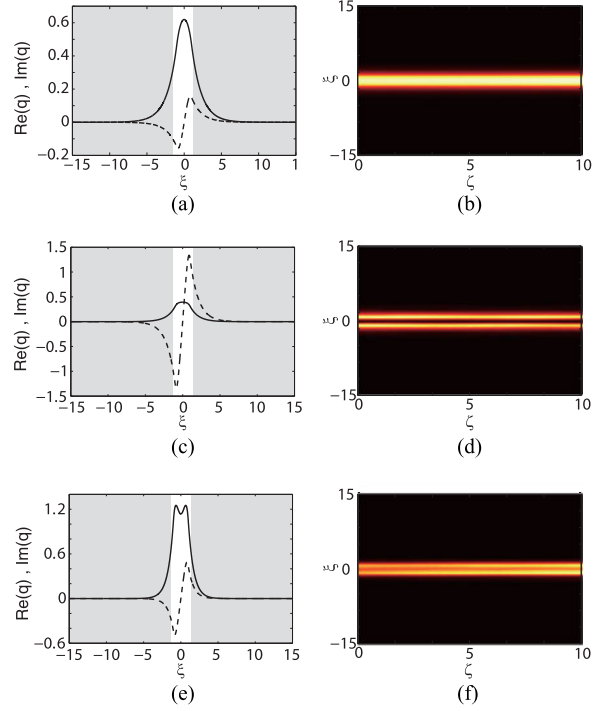


Fig. 6. (a) Real (solid line) and imaginary (dashed line) parts of the one mode regime for  $V_2 = 1$  corresponding to the propagation constant  $b_1 \approx -0.43$ . (c) and (e) Real (solid lines) and imaginary (dashed lines) parts of the modes in the two-mode configuration of the waveguide at  $V_2 = 7$ ; the modes correspond to the propagation constants  $b_2 \approx -0.17$  and  $b_1 \approx 0.93$ . The white (shaded) domain show  $|\xi| \leq 1$  ( $|\xi| > 1$ ). Stable propagation of modes is shown in the panels (b), (d), and (f), respectively. In all panels  $V_0 = -1$  and  $V_1 = 1.1$ .

nience, we set  $V_0 = -1$  and  $V_1 = 1.1$ , allowing to explore the inputs corresponding to the modes shown in Fig. 3. However now we consider variation of the coefficient  $V_2$  between two values corresponding to one-mode and two-mode realizations of the waveguide. More specifically we choose the following model of the transition:

$$V_2 = 4 + \alpha \tanh [(\zeta - \zeta_0)/\ell], \quad (13)$$

where  $\alpha$  is the amplitude of the variation of the potential,  $\zeta_0$  and  $\ell$  are the center and width (steepness) of the transition between the two domains, respectively. In particular, large values of  $\ell$  correspond to the slow (adiabatic) transition, while small  $\ell$  produces a sharp jump.

We are interested in the situation when the parameters of the regions to the left and to the right from the transition correspond to waveguides with different numbers of modes. At the output of the waveguide (i.e., at  $\zeta = 0$ ), we have  $V_2 \approx 4 - \alpha$ , while after the transition (i.e., at the waveguide output  $\zeta \gg \zeta_0$ ),  $V_2 \approx 4 + \alpha$ . Thus by choosing different (positive or negative) values of  $\alpha$  one can design a transition between different guiding regimes, like for instance, a transition from a two-mode to a one-mode regime or *vice versa*. Notice an interesting aspect of this situation: it has no discrete analogy, i.e., it cannot be reduced to two coupled waveguides (say, similar to ones studied in [33]).

### A. Adiabatic Transition Between Two Different Waveguides

We start by applying the input beams to the one-mode side at  $\zeta = 0$  and explore patterns of the transmitted beams in the domain sufficiently far from the transition region (i.e., at  $\zeta > \zeta_0$ ) where the waveguide carries two modes. This study will be referred to as the first numerical experiment. As the second numerical experiment, we apply the beam from the side where there exist two modes (two isolated eigenvalues), and analyze what comes out from the side where there is only one mode. Since we vary  $V_2$  the two sides of the waveguide correspond to two different points on the abscissa axis in Fig. 3(a).

First of all, we consider an adiabatic passage between the two domains. To define adiabaticity we recall that the modes (if they are two) are non-orthogonal, and any perturbation triggers energy exchange between them, as well as between the modes and the continuum spectrum. The characteristic distance  $Z$  of the energy exchange is determined by the differences in the eigenvalues (they are  $\sim 1$  in Fig. 3(a)), i.e.,  $Z \sim 1$ . Thus the “adiabaticity” or smoothness of the transition is determined by  $\ell \gg 1$ .

In the first numerical experiment, where the light propagates from one-mode waveguide towards the two-mode one, we do not expect significant decay of the transferred power, because after passing the transition the light can be caught by two modes (two “guiding channels”) enhancing transparency of the device. However, in the transition domain some portion of the energy can be transformed into continuous spectrum representing diffraction outwards the waveguide. On the other hand, when the light is transmitted from the two-mode to one-mode waveguide, the transition occurs to the medium with weaker guidance (since only one guiding channel is presented). In this situation, we expect a significant transfer of the energy from the guided mode to the continuous spectrum (i.e., from the discrete to continuous spectrum) and significant decay of intensity of the output field in inside the waveguide due to the diffraction.

To verify the described scenarios, we performed numerical simulations for  $\alpha = 3$ ,  $\ell = 10$ , and  $\zeta_0 = 30$  with the initial condition taken at  $\zeta = 0$  as the one-core mode (one can also consider a simple Gaussian input, which leads to a similar evolution). In the second numerical experiment, we did the same, but taking  $\alpha = -3$ . The inversion of the sign of  $\alpha$  is equivalent to swapping the positions of the one-mode and two-mode segments of the waveguide. Respectively, in the second experiment the initial condition was taken as the two-core mode.

The results of both numerical experiments are presented in Fig. 7. The results of the first simulation where the input beam in the form of the mode shown in Fig. 6(a) is applied to the “one-mode side” of the waveguide with the transition is illustrated in Fig. 7(a). As expected, we observe the almost complete transmission of the beam. After the transition, the beam is (adiabatically and almost completely) transformed into the fast mode, shown by the black solid line in Fig. 7(b), which corresponds to the background state shown in Fig. 6(e).

Next, numerical simulations were performed with the input modes applied to the “two-mode side” of the waveguide. In Fig. 7(c), we show the propagation of the slow input mode from

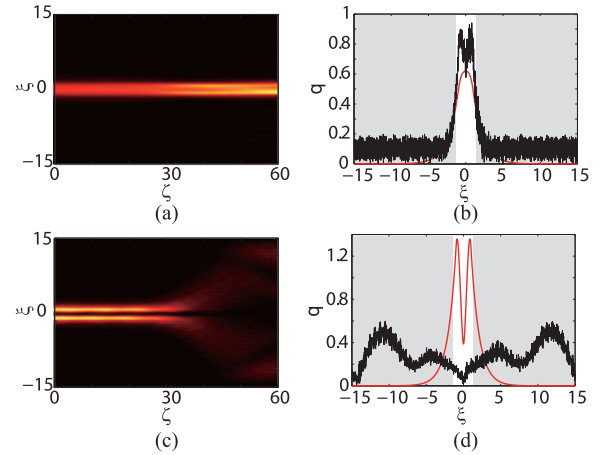


Fig. 7. (a) Propagation of a beam which at the input represents the mode shown in Fig. 6(a). (c) Propagation of a beam which at the input represents the mode shown in Fig. 6(b). (b) and (d) The spatial profiles of the input (red lines) and output fields (black lines) corresponding to (a) and (c) at  $\zeta = 60$ , respectively. In all panels  $V_0 = -1$ ,  $V_1 = 1.1$ , and  $\ell = 10$ .

Fig. 6(b) [see the red line in Fig. 7(d)]. After the transition, we observe the almost complete diffraction of the beam [see the black line in Fig. 7(d)]. The same experiment launched with the fast input mode from Fig. 6(b) gives a similar result.

Comparing the upper and lower panels in Fig. 7, we observe the expected nonreciprocal propagation of the light applied to opposite sides of the waveguide with the transition between one-to-two mode configuration. Thus the structure operates like an optical diode-like device allowing for a transmission of a beam localized near the core of the waveguide only in one direction.

The “quality” of such a “light diode,” can be characterized by the integral form-factor

$$Q = \frac{\int_{-\infty}^{\infty} |q|^4 d\xi}{\left(\int_{-\infty}^{\infty} |q|^2 d\xi\right)^2} \quad (14)$$

which is inversely proportional to the width of the pulse. Therefore, spatially localized (delocalized) distribution is characterized by a large (small) value of  $Q$ . Consequently, we find that  $Q \approx 0.25$  for the first numerical experiment [Fig. 7(a)] and  $Q \approx 0.06$  for the second numerical experiment [see Fig. 7(c)] already at  $\zeta = 60$ .

### B. Non-Adiabatic Transition Between Two Different Waveguides

The adiabaticity of the transition between the two domains of the waveguide does not appear to be important for the implementation of the diode-like behavior. In order to confirm this observation, can be useful to reduce the size of the device, we study the “non-adiabatic” transition between one-mode and two-mode regions. We explore the same structure as in Section IV-A but now with  $\ell < 1$  (to be specific, we choose  $\ell = 0.1$ ).

The results are presented in Fig. 8. The input light is caught by the emergent levels when we send the beam from the side with only one localized mode, as shown in the panel (a). However, it escapes from the waveguide when sent from the side

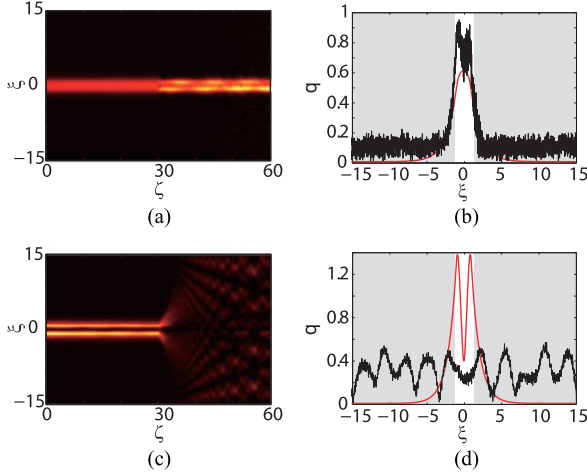


Fig. 8. (a) Propagation of the input beam in a form of the mode shown in Fig. 6(a) applied to the one-mode side of the waveguide. (c) Propagation of the input beam in a form of the mode shown in Fig. 6(b) applied to the two-mode side of the waveguide. (b) and (d) Show the spatial profiles of the field at the input (red lines) and at output fields, i.e., at  $\zeta = 60$ , and correspond to propagation shown in (a) and in (c). In all panels  $V_0 = -1$ ,  $V_1 = 1.1$ , and  $\ell = 0.1$ .

with two localized modes, as shown in the panel (c). The computed integral form-factors are  $Q \approx 0.25$  for the first numerical experiment [see Fig. 8(a)], and  $Q \approx 0.04$  for the second numerical experiment [see Fig. 8(c)] at  $\zeta = 60$ . Compared to the case of adiabatic transition (shown in Fig. 7), now we observe that the input light diffracts more strongly in the transition domain. We also observe the pronounced periodic energy transfer between the two modes after the beam passes through the transition domain (the period of the transfer is estimated as  $2\pi/(b_1 - b_2) \approx 5.7$ ). This indicates that the output beam in Fig. 8(a), (b) is a superposition of the two modes.

## V. SCATTERING BY A TUNABLE DEFECT

The phenomena governing unidirectional light propagation described above, can be also observed if the modification of the modal structure of the waveguide is implemented only in a finite region of the propagation distance in the form of a localized defect. This situation can be designed using a pair of transitions one of which is placed at  $\zeta = \zeta_0 - Z$  and another one is placed at  $\zeta = \zeta_0 + Z$ . Here the parameters  $\zeta_0 > Z$  and  $Z > 0$  characterize the center and the half-width of the defect, respectively. In this section, we will address two situations. In the first case, the regions outside the defect (i.e., for  $0 < \zeta < \zeta_0 - Z$  and  $\zeta > \zeta_0 + Z$ ) are characterized by the refractive index supporting two propagating modes, while the modified (defect) domain (i.e., for  $\zeta_0 - Z < \zeta < \zeta_0 + Z$ ) supports only one mode. In the second case, we consider an inverse situation, where the outside domains are characterized by one mode, while the defect supports two modes.

Starting with the first case, we model it by

$$V_2 = 1 + \alpha \tanh\left(\frac{\zeta - \zeta_0 + Z}{\ell}\right) - \alpha \tanh\left(\frac{\zeta - \zeta_0 - Z}{\ell}\right) \quad (15)$$

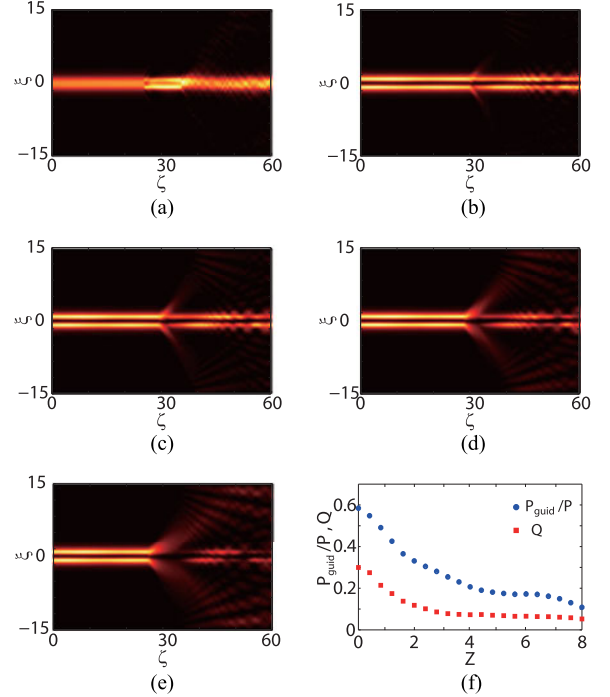


Fig. 9. (a) Scattering by a tunable defect which locally transforms a one-mode waveguide into a two-mode one. The width of the defect domain is  $2Z = 10$ . (b)–(e) Scattering by a tunable defect which locally transforms a two-mode waveguide into a one-mode regime, for  $Z = 1$  (b),  $Z = 2$  (c),  $Z = 4$  (d), and  $Z = 8$  (e), respectively. (f) Dependence of  $P_{\text{guid}}/P$  ( $P \approx 3.5$  in the whole scattering process) and  $Q$  on the half-width of the defect  $Z$ . In all panels,  $V_0 = -1$ ,  $V_1 = 1.1$ ,  $\zeta_0 = 30$ , and  $\ell = 0.1$ .

with  $\alpha = 3$ ,  $\zeta_0 = 30$ , and a small  $\ell = 0.1$  characterizing the steepness of the transition between the guiding regimes. Thus  $V_2 \approx 1$  at the input and at the output of the waveguide, and  $V_2 \approx 1 + 2\alpha = 7$  inside the defect (e.g., at  $\zeta = \zeta_0$ ). Considering a localized pulse at the input, we have scanned the range  $0.1 \leq Z \leq 20$ . As was explained above [see the discussion of Fig. 3(b)], the real part of the refractive index significantly increases and number of supported modes is changed to two. This facilitates light propagation as two channels are now open. It is thus natural that the input light remains localized after the interaction with the defect no matter its width is small ( $Z$  is close to 0.1) or large ( $Z$  is close to 20) compared with the width of the incident pulse. A typical example of the transmission is shown in Fig. 9(a), and the half-distance between the defects is  $Z = 5$ .

We have also computed the power in the guided mode defined as

$$P_{\text{guid}} = \int_{-1}^1 |q|^2 d\xi. \quad (16)$$

Thus the power of the evanescent field  $P_{\text{evan}} = P - P_{\text{guid}}$ , with the total power  $P = \int_{-\infty}^{\infty} |q|^2 d\xi$ . For the scattering in Fig. 9(a), we have  $P_{\text{guid}} \approx 0.7$  for the input mode. In the defect domain, where the waveguide can carry two modes, we observe that  $P_{\text{guid}}$  increases by about 40% (i.e.,  $P_{\text{guid}} \approx 1.0$ ). After passing through the defect,  $P_{\text{guid}}$  decreases slightly as a small part of energy is transferred to the continuous spectrum and diffracts.

Turning now to the second case of a one-mode defect embedded into a two-mode waveguide, we explore the model

$$V_2 = 7 + \alpha \tanh\left(\frac{\zeta - \zeta_0 + Z}{\ell}\right) - \alpha \tanh\left(\frac{\zeta - \zeta_0 - Z}{\ell}\right), \quad (17)$$

with  $\alpha = -3$ ,  $\zeta_0 = 30$ , and  $\ell = 0.1$ . Thus  $V_2 \approx 7$  at the input and at the output of the waveguide, and  $V_2 \approx 7 + 2\alpha = 1$  inside the defect (e.g., at  $\zeta = \zeta_0$ ). In Fig. 9(b)–(e), we show scattering for different values of  $Z$ . Now inside the defect light propagation is allowed only in one mode, which results in the strong scattering. In this case, the input light remains localized only if the width of the defect  $2Z$  is small, although even for small  $Z$  the diffraction pattern outside the waveguide is still visible [see Fig. 9(b)]. By increasing the width of the defect, we observe relatively fast decay of the form-factor  $Q$  and the power in the guided mode  $P_{\text{guid}}$ . When the input and transmitted beams are close to the exact eigenmode solutions, the total power changes weakly, in spite of the gain and loss domains; in our simulations  $P \approx 3.5$  along the whole scattering process. Thus the decay of the power inside the waveguide results from the energy transfer to the continuous spectrum. This is illustrated in panels (c), (d), and (e) of Fig. 9. In panel (f), we show the functions of  $P_{\text{guid}}/P$  and  $Q$  with respect to the half-width of the defect  $Z$ .

Thus, one can control the width of the defect region to increase or to decrease the light intensity at the output. Namely, by increasing the defect width one can strongly decrease the light intensity, which can be viewed as “switching off” the light. On the contrary, by decreasing the defect width one can preserve almost completely light energy into guided mode, which can be viewed as “switching on” the light.

## VI. TRANSITION THROUGH A FIXED DEFECT

Now we turn to the model (12) and consider interaction of the beam with change of the wave waveguide mode structure created by the external fixed defects (i.e., in the situation which is schematically presented in Fig. 2(b)). Additionally, we intend to explore the situation where number of modes involved is larger than two. To this end, we fix the parameters  $(V_1, V_2) = (1.1, 7)$  and model a fixed defect by

$$V_0 = -1 + \alpha \tanh\left(\frac{\zeta - \zeta_0 + Z}{\ell}\right) - \alpha \tanh\left(\frac{\zeta - \zeta_0 - Z}{\ell}\right), \quad (18)$$

with  $\alpha = -7$ ,  $\zeta_0 = 30$ , and  $\ell = 0.1$ . Thus at the input and at the output of the waveguide we have  $V_0 \approx -1$ , while in the region of the defect  $V_0 \approx -1 + 2\alpha = -15$ . From Fig. 5, we observe that this situation corresponds to a three-mode segment of the width  $2Z$  embedded into a two mode waveguide. For the input beam, we use the initial condition in a form of the mode shown in Fig. 6(c).

In Fig. 10(a)–(d), we show the results of the scattering by defects of different sizes. Similarly to the results obtained above [cf., Fig. 9(a)], the defect region carries more modes than the waveguide itself and transmits the beam. However, the fixed defect does not lead to scattering into the continuous spectrum

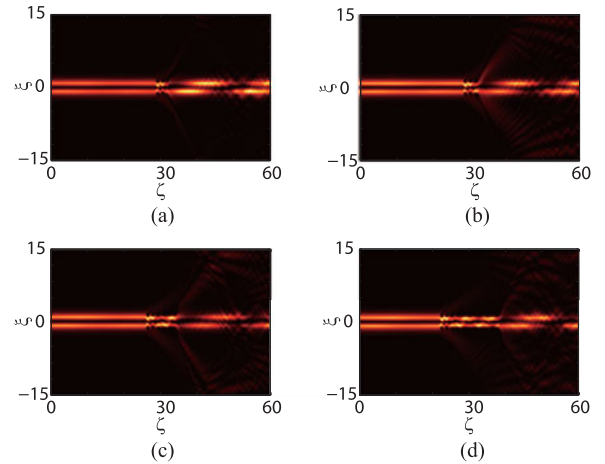


Fig. 10. Propagation of the beam in a two-mode waveguide with a fixed defect (cladding defect) which creates a localized inclusion carrying three modes. The half-width of the defect is  $Z = 1$  (a),  $Z = 2$  (b),  $Z = 4$  (c), and  $Z = 8$  (d), respectively. In all panels,  $V_1 = 1.1$ ,  $V_2 = 7$ , and  $\ell = 0.1$ .

[cf., Figs. 10 and 9], in spite of the sharp transition (small  $\ell$ ) and even for large defect width. We found that  $P_{\text{guid}}$  increases in the defect domain and decreases after passing through the defect. We also found that in the defect region, as well as at the waveguide output there is appreciable energy exchange among three and two modes, respectively. This energy transfer is faster in the defect region where the structure guides three modes.

## VII. SCATTERING BY A $\mathcal{PT}$ -SYMMETRY BREAKING DEFECT

Returning to tunable defects, we study the scattering of a light beam by a defect which locally breaks the  $\mathcal{PT}$  symmetry. This occurs in the vicinity of the center of the defect region, i.e., in the vicinity of  $\zeta_0$ . This statement is similar to that studied in [33] where a coupler governed by two coupled  $\mathcal{PT}$ -symmetric nonlinear Schrödinger equations was considered. The present model, however, has two essential differences as compared to the one studied in [33]: (i) now we model the two-core waveguide by a single (linear) equation, i.e., inter-channel coupling is accounted exactly, rather than in the tight-binding approximation as in [33], and (ii) as a consequence, now there is continuous spectrum describing diffraction of the beam. This last point is relevant because it represents a “channel” for the energy escape from the waveguide which is not related to the dissipation inside the waveguide.

To model the described situation, we modify the complex part of the dielectric permittivity, i.e.,  $V_1(\zeta)$  using the analysis of the mode structure presented in Fig. 4. More specifically, we take

$$V_1 = 1 + \frac{1}{2} \tanh\left(\frac{\zeta - \zeta_0 + Z}{\ell}\right) - \frac{1}{2} \tanh\left(\frac{\zeta - \zeta_0 - Z}{\ell}\right) \quad (19)$$

with  $\zeta_0 = 30$  and  $\ell = 0.1$  (i.e.,  $V_1 \approx 1$  at the input and at the output of the waveguide, and  $V_2 \approx 2$  at the center of the segment with the broken  $\mathcal{PT}$  symmetry at  $\zeta_0 = 30$ ). As before, the half-width of the defect,  $Z$ , is considered as a control parameter.



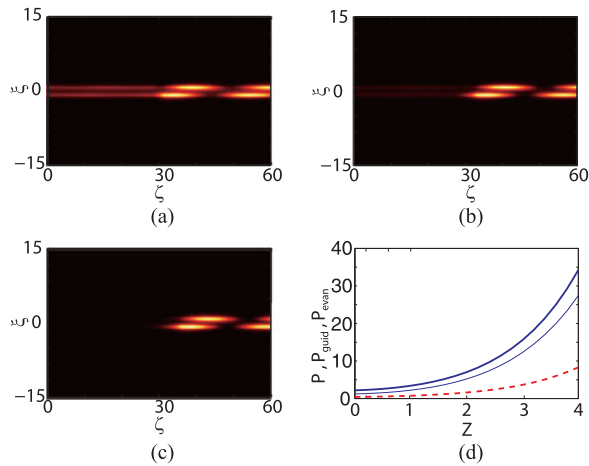


Fig. 11. (a)–(c) Scattering by a  $\mathcal{PT}$ -symmetry breaking defect for  $Z = 1, 2$ , and 4, respectively. A periodic energy transfer between the two cores is clearly observed. (d) The total power  $P$  (thick solid line), the guided power  $P_{\text{guid}}$  (thin solid line), and the diffracted power  $P_{\text{cont}}$  (dashed line) as functions of the defect width  $2Z$ .

In Fig. 11, we present typical results of the numerical simulations of the described setting. In panels (a)–(c) we show the dynamics for three different widths of the defect. The initial condition is chosen as an eigenmode with  $(V_0, V_1, V_2) = (-1, 1, 10.5)$  and propagation constant  $\approx 0.9$ , see Fig. 4(a). After the beam passes the first defect and enters the region with the broken  $\mathcal{PT}$  symmetry the intensity grows exponentially. This growth stops after the beam passes the defect and returns to the guiding regime with the unbroken  $\mathcal{PT}$  symmetry. The further evolution is accompanied by periodic energy transfer between the two cores, occurring due to the nonorthogonality of the modes. The output intensity grows exponentially with the distance between the defects, as shown in Fig. 11(d). Here we observe increase of the total power  $P$  and of the power in the guided mode  $P_{\text{guid}}$ , whereas the power in the diffracting wave  $P_{\text{cont}}$  increases much slower. The period of the energy transfer is not sensitive to the defect size. Thus as a matter of fact we observe that the waveguide operates as an effective *amplifier* of the beam.

### VIII. DISCUSSION AND SUMMARY

In this paper, we described a scheme allowing one to create a  $\mathcal{PT}$ -symmetric optical waveguide whose parameters and even mode structure can be varied in space at will. The system consists of a mixture of two isotopes of  $\Lambda$ -type atomic gas loaded in a cell with Bragg cladding and exposed to several laser fields with Raman excitations. A  $\mathcal{PT}$ -symmetric refractive index can be induced by manipulating the real and imaginary parts of the refractive index of the system.

We have demonstrated that by modulating system parameters such various functional regimes of the device can be implemented. In particular, properly designed waveguide allows for transitions between waveguide configurations supporting different numbers of guiding modes, as well as two types of defects: tunable ones created by local change of refractive index inside

the waveguide, and fixed ones created by the local change of the property of the Bragg cladding. We have found that local (or extended) change of the waveguide towards an increase of the number of guiding modes supports and even enhances light propagation. Otherwise, if a defect or transition results in a reduction of the number of guiding modes, a strong attenuation of guided beams can be observed. Consequently, the  $\mathcal{PT}$ -symmetric optical waveguide with these defects can be used to design optical diode-like devices, switches, or amplifiers.

We emphasize that the feasibility of the scheme is based on already well elaborated experimental techniques on designing the dielectric susceptibility of atomic vapor cells [6], [7], [35], [36] as well as on practical availability of hollow-core waveguides having wide range of parameters and diverse technical parameters (e.g., planar waveguides with Bragg mirrors [37] or more sophisticated hollow-core photonic bandgap fibers [38]). Also, it worth also mentioning that the proposed scheme is structurally stable, i.e., small deviations of system parameters do not break the obtained  $\mathcal{PT}$  symmetry. In fact, although the accuracy of the  $\mathcal{PT}$  symmetry becomes lower, the unidirectional propagation and other functionalities persist until changes of the system parameters exceed 10% of their exact values in the  $\mathcal{PT}$ -symmetric configuration.

### REFERENCES

- [1] L. V. Hau, S. E. Harris, Z. Dutton, and C. H. Behroozi, "Light speed reduction to 17 metres per second in an ultracold atomic gas," *Nature* vol. 397, pp. 594–598, 1999.
- [2] M. D. Lukin, P. R. Hemmer, M. Löffler, and M. O. Scully, "Resonant enhancement of parametric processes via radiative interference and induced coherence," *Phys. Rev. Lett.*, vol. 81, 1998, Art no. 2675.
- [3] C. Liu, Z. Dutton, C. H. Behroozi, and L. V. Hau, "Observation of coherent optical information storage in an atomic medium using halted light pulses," *Nature*, vol. 409, pp. 490–493, 2001.
- [4] D. F. Phillips, A. Fleischhauer, A. Mair, R. L. Walsworth, and M. D. Lukin, "Storage of light in atomic vapor," *Phys. Rev. Lett.*, vol. 86, 2001, Art no. 783.
- [5] M. O. Scully, "Enhancement of the index of refraction via quantum coherence," *Phys. Rev. Lett.*, vol. 67, 1991, Art no. 1855.
- [6] D. D. Yavuz, "Refractive index enhancement in a far-off resonant atomic system," *Phys. Rev. Lett.*, vol. 95, 2005, Art no. 223601.
- [7] N. A. Proite, B. E. Unks, J. T. Green, and D. D. Yavuz, "Refractive index enhancement with vanishing absorption in an atomic vapor," *Phys. Rev. Lett.*, vol. 101, 2008, Art no. 147401.
- [8] C. Hang, G. Huang, and V. V. Konotop, " $\mathcal{PT}$  symmetry with a system of three-level atoms," *Phys. Rev. Lett.*, vol. 110, Art no. 083604, 2013.
- [9] C. Hang, D. A. Zezyulin, V. V. Konotop, and G. Huang, "Tunable nonlinear parity-time-symmetric defect modes with an atomic cell," *Opt. Lett.*, vol. 38, pp. 4033–4036, 2013.
- [10] C. Hang, D. A. Zezyulin, G. Huang, V. V. Konotop, and B. A. Malomed, "Tunable nonlinear double-core  $\mathcal{PT}$ -symmetric waveguides," *Opt. Lett.*, vol. 39, Art no. 5387, 2014.
- [11] J. Sheng, M.-A. Miri, D. N. Christodoulides, and M. Xiao, " $\mathcal{PT}$ -symmetric optical potentials in a coherent atomic medium," *Phys. Rev. A*, vol. 88, Art. no. 041803(R), 2013.
- [12] H.-J. Li, J.-P. Dou, and G. Huang, "PT symmetry via electromagnetically induced transparency," *Opt. Exp.*, vol. 21, Art. no. 32053, 2013.
- [13] R. El-Ganainy, K. G. Makris, D. N. Christodoulides, and Z. H. Musslimani, "Theory of coupled optical PT-symmetric structures," *Opt. Lett.*, vol. 32, pp. 2632–2634, 2007.
- [14] C. M. Bender and S. Boettcher, "Real spectra in non-hermitian hamiltonians having PT symmetry," *Phys. Rev. Lett.*, vol. 80, Art. no. 5246, 1998.
- [15] C. M. Bender, "Making sense of non-Hermitian Hamiltonians," *Rep. Prog. Phys.*, vol. 70, no. 6, Art. no. 947, 2007.

- [16] R. Y. Chiao, "Superluminal (but causal) propagation of wave packets in transparent media with inverted atomic populations," *Phys. Rev. A*, vol. 48, Art. no. R34, 1993.
- [17] A. Ruschhaupt, F. Delgado, and J. G. Muga, "Physical realization of PT-symmetric potential scattering in a planar slab waveguide," *J. Phys. A*, vol. 38, Art. no. L171, 2005.
- [18] C. E. Rüter *et al.*, "Observation of parity-time symmetry in optics," *Nature Phys.*, vol. 6, pp. 192–195, 2010.
- [19] B. Peng *et al.*, "Parity-time-symmetric whispering-gallery microcavities," *Nature Phys.*, vol. 10, pp. 394–398, 2014.
- [20] L. Chang *et al.*, "Parity-time symmetry and variable optical isolation in active-passive-coupled microresonators," *Nature Photon.*, vol. 8, pp. 524–529, 2014.
- [21] H. Ramezani, T. Kottos, R. El-Ganainy, and D. N. Christodoulides, "Unidirectional nonlinear PT-symmetric optical structures," *Phys. Rev. A*, vol. 82, Art. no. 043803, 2010.
- [22] Z. Lin *et al.*, "Unidirectional invisibility induced by PT-Symmetric periodic structures," *Phys. Rev. Lett.*, vol. 106, Art. no. 213901, 2011.
- [23] L. Feng *et al.*, "Experimental demonstration of a unidirectional reflectionless parity-time metamaterial at optical frequencies," *Nature Mater.*, vol. 12, pp. 108–113, 2013.
- [24] M. Scalora, J. P. Dowling, C. M. Bowden, and M. J. Bloemer, "The photonic band edge optical diode," *J. Appl. Phys.*, vol. 76, Art. no. 2023, 1994.
- [25] M. D. Tocci *et al.*, "Thin film nonlinear optical diode," *Appl. Phys. Lett.*, vol. 66, pp. 2324–2326, 1995.
- [26] V. V. Konotop and V. Kuzmiak, "Nonreciprocal frequency doubler of electromagnetic waves based on a photonic crystal," *Phys. Rev. B*, vol. 66, Art. no. 235208, 2002.
- [27] N. Li and J. Ren, "Non-reciprocal geometric wave diode by engineering asymmetric shapes of nonlinear materials," *Sci. Rep.*, vol. 4, p. 6228, 2014.
- [28] D.-W. Wang *et al.*, "Optical diode made from a moving photonic crystal," *Phys. Rev. Lett.*, vol. 110, 2013, Art. no. 093901.
- [29] D. Steck, <sup>85</sup>Rb D Line Data [Online]. Available: <http://steck.us/alkalidata>
- [30] R. W. Boyd, *Nonlinear Optics*. Amsterdam, The Netherlands: Elsevier, 2008.
- [31] B. Meng and Q. J. Wang, "Broadly tunable single-mode mid-infrared quantum cascade lasers," *J. Opt.*, vol. 17, Art. no. 023001, 2015.
- [32] L. Grigory, H. Andreas, K. Sven, and O. Stefan, "LCOS spatial light modulators: Trends and applications," in *Optical Imaging and Metrology Advanced Technologies*. Weinheim, Germany: Wiley-VCH, 2012.
- [33] Y. V. Bludov, C. Hang, G. Huang, and V. V. Konotop, "PT-symmetric coupler with a coupling defect: Soliton interaction with exceptional point," *Opt. Lett.*, vol. 39, pp. 3382–3385, 2015.
- [34] F. K. Abdullaev, V. V. Konotop, M. Öggen, and M. P. Sørensen, "Zeno effect and switching of solitons in nonlinear couplers," *Opt. Lett.*, vol. 36, pp. 4566–4568, 2011.
- [35] S. E. Harris, "Refractive-index control with strong fields," *Opt. Lett.*, vol. 19, pp. 2018–2020, 1994.
- [36] A. S. Zibrov *et al.*, "Experimental demonstration of enhanced index of refraction via quantum coherence in Rb," *Phys. Rev. Lett.*, vol. 76, pp. 3935–3938, 1996.
- [37] A. W. Snyder and J. Love, *Optical Waveguide Theory*. New York, NY, USA: Springer, 1983.
- [38] F. Benabid, "Hollow-core photonic bandgap fibre: New light guidance for new science and technology," *Philosoph. Trans. R. Soc. A*, vol. 364, pp. 3439–3462, 2006.



ear optical waves in atomic gas and nonlinear matter waves in Bose–Einstein condensates.



**Dmitry A. Zezyulin** received the M.S. degree in applied mathematics from the Moscow Institute of Electronic Technology, Moscow, Russia, in 2006, and the Ph.D. degree in mathematical modeling from the Institute of Mathematical Modeling of Russian Academy of Sciences, Moscow, in 2009. Then he became a Postdoctoral Research Fellow at the University of Lisbon, Lisbon, Portugal. He studies stationary linear and nonlinear modes in Bose–Einstein condensates, optics, and parity-time-symmetric systems.



micronanostructures.

**Guoxiang Huang** received the M.S. degree in theoretical physics from Xiangtan University, Hunan, China, in 1987, and the Ph.D. degree in theoretical physics from Fudan University, Shanghai, China, in 1991. He became an Assistant Professor at the Department of Physics, Xiangtan University, in 1988, and an Associate Professor and a full Professor at the Department of Physics, East China Normal University, Shanghai, China, respectively, in 1992 and 1994. His research interests include nonlinear and quantum interference effects in atoms, molecules, and



at the Department of Physics at the Faculty of Sciences. His research interests include nonlinear wave phenomena in optics, in Bose–Einstein condensates, and discrete systems.